Growth of Co isolated clusters in the gas phase: Experiment and molecular dynamics simulations

Sébastien Rives,[1] Alain Catherinot,[1] Frédéric Dumas-Bouchiat,[1] Corinne Champeaux,[1]
Arnaud Videcoq,[2] and Riccardo Ferrando[3]
[1]*SPCTS UMR CNRS 6638, Faculté des Sciences, 123 Avenue Albert Thomas, 87060 Limoges Cedex, France*
[2]*SPCTS UMR CNRS 6638, ENSCI, 47 Avenue Albert Thomas, 87065 Limoges Cedex, France*
[3]*Dipartimento di Fisica, Università di Genova, Via Dodecaneso 33, 16416 Genova, Italy*
(Received 11 July 2007; revised manuscript received 23 November 2007; published 5 February 2008)

The structures of cobalt clusters are investigated by simulations and experiments. The growth process of isolated clusters in gas phase is simulated by molecular dynamics, growing clusters atom by atom from a small seed up to the size of 600 atoms. Experimentally, clusters are generated by a laser ablation cluster generator using low energy clusters beam deposition. Then, the deposited aggregates are characterized with high resolution transmission electronic microscope. Simulation results are compared with the experiment, and with previous density functional theory and semiempirical calculations, obtaining a good agreement both for the geometric structures and for the behavior of lattice contraction. Finally, aggregation simulations are performed to determine the nucleation rate of cobalt monomers.

DOI: 10.1103/PhysRevB.77.085407 PACS number(s): 61.46.Bc, 36.40.Sx, 81.10.Bk, 71.15.Pd

I. INTRODUCTION

Nanoscale clusters are of great interest for basic science and applications since they display peculiar physical and chemical properties, which are qualitatively different from those of isolated atoms and of bulk materials.[1,2] Applications are possible in several contexts. For example, matrix-embedded nanoclusters[3] find applications in optics. Clusters of transition metals such as Ni, Co, or Fe achieve the goal of catalyst for the growth of carbon nanotubes.[4] When injected in a liquid,[5] nanoclusters can produce a magnetic fluid.

When studying the nanoclusters properties, the first step is the determination of their structure. This is a nontrivial task since nanoclusters can present a large variety of structures[1] pertaining to different motifs. In fact, clusters can exhibit "noncrystallographic" structures such as icosahedra (Ih) or decahedra (Dh).[6] There are cases in which clusters present crystallographic structures which are different from the structure of the bulk material. A well known example is cobalt: bulk cobalt is usually (at room temperature and pressure) hexagonal close-packed (hcp), while 3 nm radius Co clusters present face centered cubic (fcc) facets.[7] Several physical sources have been developed for clusters synthesis, e.g., the Slatter method,[8] pulsed arc cluster ion sources,[9] dc magnetron sources,[10] liquid metal ion sources,[11] and laser ablation sources.[12,13]

Among the numerical methods for simulating cluster growth between 10 and 1000 atoms, molecular dynamics (MD) methods within an atom-atom potential model present some advantages with respect to Monte Carlo or *ab initio* methods. In fact, compared to Monte Carlo, MD produces physically meaningful trajectories since it solves the equations of motion. Compared to *ab initio* calculations, MD allows the study of larger cluster sizes on much longer time scales,[14] and a much more complete exploration of the cluster configuration space.[15,16] On the other hand, semiempirical models may suffer of limited accuracy. Indeed, their accuracy is strongly material dependent, so that these models must be carefully tested case by case.

In this paper, we present results of MD simulations of the growth of isolated cobalt clusters in the range of 4–600 atoms. The interplanar distance is computed depending on clusters size, finding an increase with size. These simulation results are compared with experimental data obtained by producing cobalt clusters in a laser vaporization source, and with the outcome of previous semiempirical and density-functional theory (DFT) calculations. These comparisons serve as a validation of our model. Finally, the nucleation of cobalt clusters in a vapor at constant temperature is simulated.

II. NUMERICAL METHODS AND PROCEDURES

In our MD simulations, the classical Newton's equation of motion is integrated for each cobalt atom,

$$m\frac{\delta v_i}{\delta t} = \sum_{j=1}^{N} \nabla V_{ij}, \tag{1}$$

where v_i is the velocity vector of the atom i and V_{ij} the interaction potential between the atoms i and j. In order to discretize this equation, a first order Verlet[17] algorithm with a constant time step of 7 fs has been chosen. The potential used to simulate the interaction between cobalt atoms is a Gupta potential,[18]

$$V_{ij} = \sum_{i=1}^{N}\left[\sum_{j=1,j\neq i}^{N} V_{ij}^{r}(r_{ij}) - \sqrt{\sum_{j=1,j\neq i}^{N} V_{ij}^{m}(r_{ij})}\right], \tag{2a}$$

$$V_{ij}^{r} = A\exp\left(-p\left[\frac{r_{ij}}{r_0}-1\right]\right), \tag{2b}$$

$$V_{ij}^{m} = \xi^2\exp\left(-2q\left[\frac{r_{ij}}{r_0}-1\right]\right). \tag{2c}$$

The parameters (A, p, q, and ξ) are fitted to bulk experimental values: cohesive energy, lattice parameter, and elastic

constants.[19] The values used in the following are $A=0.1757$ eV, $\xi=1.8430$ eV, $r_0=1.25$ Å, $p=9.21$, and $q=2.975$. In order to maintain a constant temperature during the simulation, an Andersen thermostat[20] has been employed. Since the model potential has been fitted to bulk quantities, there is no warranty that it would be accurate for nanoclusters, in which many atoms are undercoordinated. However, the semiempirical approach has been fruitful for several transition and noble metal clusters,[1,21] so that we are confident that it can be useful for cobalt too. We remark also that the structures found by semiempirical studies serve as a starting point for structural relaxation by means of more sophisticated (but much more cumbersome) techniques.[22,23]

Rodríguez-López *et al.*[24] optimized Co clusters within the same type of semiempirical model,[18] but with a different parametrization. Even though their parameter values are quite different from ours, the product pq, which is the main quantity ruling the crossover sizes between structural motifs,[21] is very close. In the following, we shall compare our results with those of Rodríguez-López *et al.* for small clusters which are more reliable for establishing the correct energetic ordering of isomers.

Two different growth simulation types have been implemented, the first for the search of the growth structures of clusters from 4 to 600 atoms, and the second for the investigation of cluster nucleation in metallic vapor. In the first simulation type, a single cluster is grown at a time by adding atoms on a small seed.[14] Atoms are added one by one at a deposition rate of one atom each 7 ns. In between two depositions, the cluster evolves at the constant temperature of 600 K.

Each nanosecond, local minimization runs are performed, and the locally minimized structures are retained. The structures obtained in the growth simulations are analyzed by taking snapshots each picosecond. For each snapshot, common neighbor analysis[25] signatures and the cluster symmetry group are determined.

The second simulation type aims at determining the dependence of the nucleation rate on temperature and vapor pressure. To this purpose, a gas of 1000 cobalt monomers is evolved at given temperature and density for 10 ns. After this thermalization period, we determine the cluster size distribution as a function of time. In the following, we report the evolution of the density of monomers J_1, of small clusters (from the dimer to the decamer) $J_s=\Sigma_{j=2}^{10}J_j$, and of clusters bigger than the decamer $J_b=\Sigma_{j=11}^{\infty}J_j$. The growth of a cluster is caused by the adsorption of monomers on its surface as well as by the coalescence with other clusters. The nucleation rate is defined as $\zeta=-\delta J_1/\delta t$. Eight different temperatures are considered.

III. EXPERIMENTAL DETAILS

The cluster generator is a laser vaporization source described in details elsewhere[26] and derived from the Smalley principle[27,28] and the Milani–de Heer design.[29] The target of cobalt is irradiated with a pulsed excimer laser (248 nm). The plume of evaporated species is quickly cooled down through interaction with helium gas, released by an electromagnetic valve with the aperture synchronized with the laser pulse. As a result of very fast cooling, the cobalt atoms and ions condensate into very small clusters. The gas-cluster mixture is squeezed out through a nozzle into the ultra high vacuum (UHV) chamber of a conventional pulsed laser deposition (PLD) system. According to this process, cluster sizes can be adjusted by varying the upstream helium pressure, the laser-valve triggering delay, the laser fluence, and the nozzle design. The substrate is held perpendicularly to the axis of the cluster beam. It is well known that very small clusters are extremely reactive. So as to prevent oxidation, the samples are shielded by a protective thin carbon film of 5 nm deposited by conventional PLD in the main UHV chamber before any further exposition to ambient atmosphere.

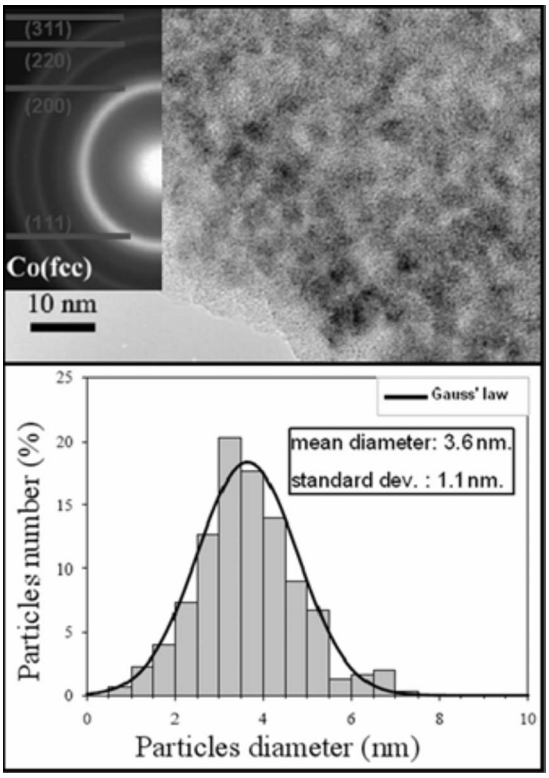

FIG. 1. Top: TEM picture of a 20 nm layer of cobalt clusters. Inset: diffraction pattern. Bottom: clusters size distribution.

The clusters which impact on the substrate placed in the chamber are expected to preserve their in-flight crystallinity. In fact, at the nozzle exit, the averaged kinetic energy per cobalt atom in the aggregates, $\bar{E}_c$, is estimated to be less than 0.5 eV.[30] This is an order of magnitude smaller than the cohesion energy of cobalt atom in the bulk. Such $\bar{E}_c$ value characterizes a low energy cluster beam deposition regime.[31]

IV. RESULTS

A. Experimental results

For transmission electron microscope (TEM) investigations, a carbon coated copper grid is directly used as a sub-

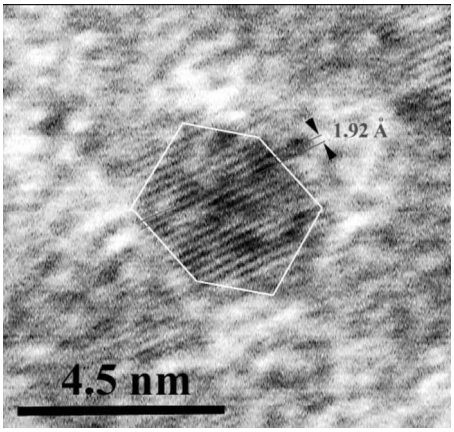

FIG. 2. HRTEM image of a 3 nm cobalt cluster with fcc(111) planes.

strate during cluster deposition. The TEM used is a JEOL 2010 operating at 200 kV. Figure 1 shows a TEM picture of a coating of cobalt aggregates. The coating is about 20 nm thick. The diffraction pattern shows the fcc structure of these small entities of cobalt. Note that, in normal conditions, the cobalt bulk structure is hexagonal close packed. An image analysis returns an average aggregate size of about 3.6 nm in diameter with a standard deviation of 1.1 nm, corresponding to cluster sizes in the range between 10^2 and 10^4 atoms.

A high resolution TEM picture of an isolated cluster is shown in Fig. 2. This cluster seems faceted and has a diameter of about 3 nm. Moreover, the measurement of the distance between the stripes, equivalent to a distance between

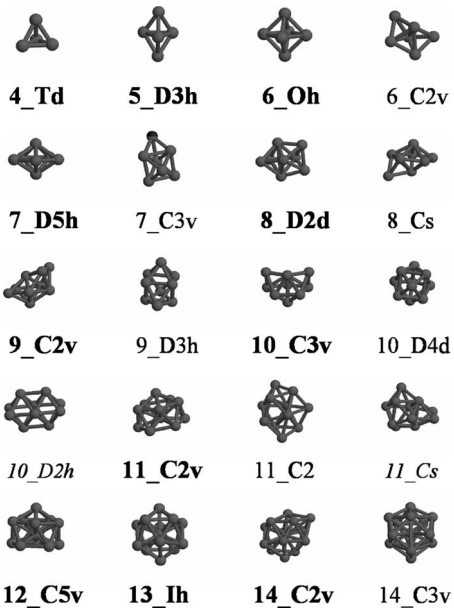

FIG. 3. Clusters structures in the size interval $4 \leqslant N \leqslant 14$ as obtained in the growth simulations. The lowest-energy isomers as well as some higher isomers are presented for some sizes. The symmetry group is specified for each cluster: in bold for lowest-energy isomers, in roman for second isomers, and in italic for third isomers.

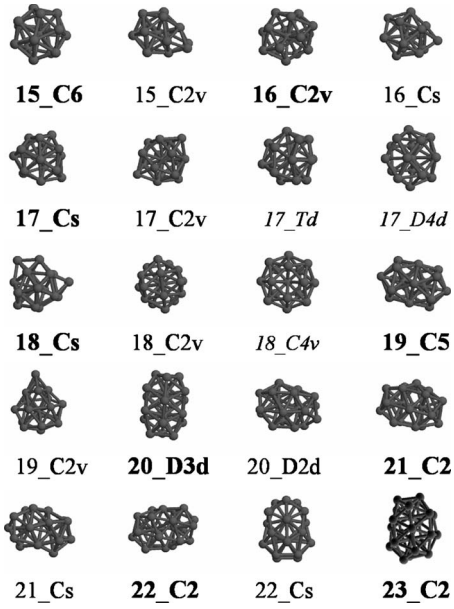

FIG. 4. Clusters structures in the size interval $15 \leqslant N \leqslant 23$ as obtained in the growth simulations. The lowest-energy isomers as well as some higher isomers are presented for some sizes. The symmetry group is specified for each cluster: in bold for lowest-energy isomers, in roman for second isomers, and in italic for third isomers.

atomic planes, gives a value of 1.92 Å ± 5%.

We may compare this distance with the distance between (111) planes in bulk fcc cobalt, which is equal to 2.05 Å. Some lattice parameter contraction seems thus to occur in nanoparticles. In the following, this contraction of interatomic distances will be checked numerically.

B. Calculated structures and comparison with experiment

1. Crystallographic structure

Representative structures of the cobalt clusters obtained in our growth simulations in the size range from 4 to 600 atoms at a temperature of 600 K are shown in Figs. 3–5. At each size considered in the figures, we show the lowest-energy isomer found in the growth simulations; for some sizes, also higher-energy isomers are shown.

For many sizes, the structure of the lowest isomer is as expected. For example, we find icosahedral structures at the magic sizes 13, 55, and 147 atoms as well as the truncated decahedral structure for 75 atoms and the truncated icosahedral structure for 146 atoms. An interesting exception is size 38, at which we do not find the usual truncated-octahedral fcc structure but a structure with D_{4h} symmetry, as depicted in Fig. 6. The origin of this structure will be discussed in the following.

For small sizes, we could expect that our growth simulations will follow the pattern of the most stable structures from the thermodynamic point of view, while when size increases kinetic trapping phenomena[1] become more and more likely, so that growth structures may become very different from thermodynamic equilibrium structures. In the small-

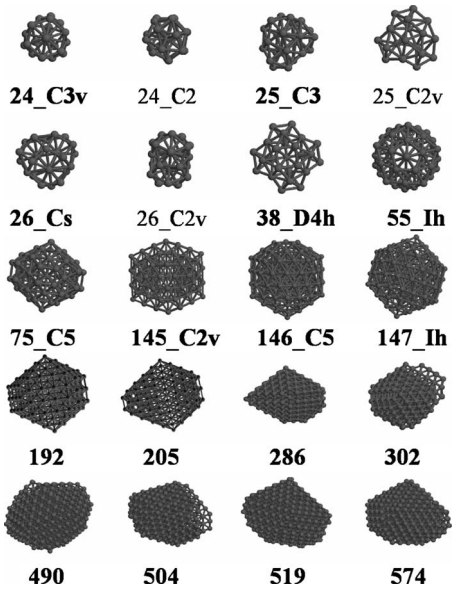

FIG. 5. Clusters structures in the size interval $N \geqslant 24$ as obtained in the growth simulations. The lowest energy isomers as well as some higher isomers are presented for some sizes. The symmetry group is specified for each cluster: in bold for lowest-energy isomers, in roman for second isomers, and in italic for third isomers.

size range, it is thus interesting to compare our growth structures with those found by Rodríguez-López *et al.*[24] as lowest-energy isomers by genetic global optimization. This comparison indicates that, even though the potential parameters used by Rodríguez-López *et al.* are different from ours, most of the lowest-energy isomers present the same structure. In fact, for sizes $N \leqslant 14$, we obtain the same isomers, and also for $N=19$, 26, and 55. The structure for 26 atoms is a polyicosahedron.[32] For size 38, our growth simulations do not find the truncated octahedron, and thus they seem in disagreement with the results of Rodríguez-López *et al.* Our structure is made of four interpenetrating 13-atom icosahedra, capped by two square facets of four atoms. However, the disagreement is only apparent. Indeed, we have verified by parallel-walker global optimization,[33] which the truncated octahedron is the global minimum also in our case. Therefore, the structure that we find for size 38 is the result of a kinetic trapping phenomenon during growth.[1] In fact, it has been shown that also in Ag and Cu,[34] the 38-atom truncated octahedron is quite difficult to obtain in a growth process because it is the only crystalline exception in a sequence of noncrystalline structures.

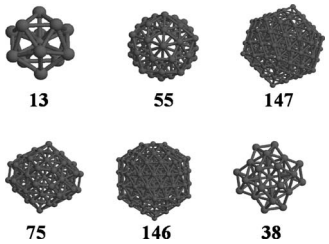

FIG. 6. Optimized structures at magic numbers.

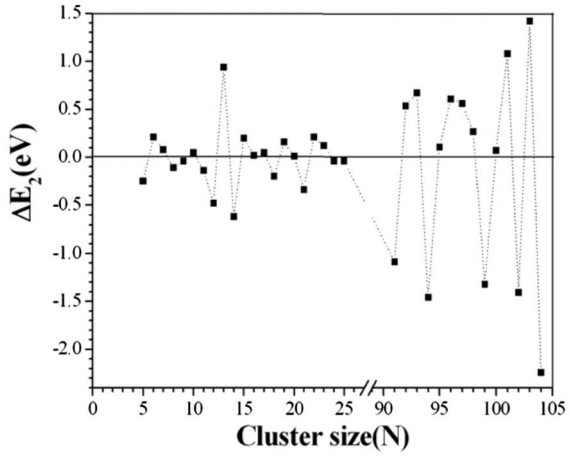

FIG. 7. Second difference in the energy [Eq. (3)] for the best isomers found in the growth simulations.

In summary, the lowest-energy structures of our model and those found by Rodríguez-López *et al.* coincide to a great extent. This confirms that cluster geometries are mainly ruled by the product pq, whose values are very close in these models.

Our structures compare well also with those found by Ma *et al.*[35] by density-functional theory calculations in the range $4 \leqslant N \leqslant 13$. In fact, we find the same lowest-energy geometries as Ma *et al.* for $N=5$, 6, 8, 12, and 13, while for $N=7$, the structure of Ma *et al.* is our second isomer. We have calculated also the second difference in the energy Δ_2,

$$\Delta_2 = -2E(N) + E(N-1) + E(N+1). \tag{3}$$

The results are reported in Fig. 7. At small sizes, we single out 6, 10, and 13 as magic numbers, to be compared with 6, 10, and 12 found by Ma *et al.*

For larger sizes, kinetic trapping phenomena[1] become more and more likely, so that growth structures may often become different from thermodynamic equilibrium structures. This is very likely for sizes greater than 200 atoms. Here, we obtain prolate structures exhibiting mostly close-packed (111)-like facets. Very often, islands in hcp stacking nucleate on the (111) faces, as can be seen in Fig. 8. The nucleation of such islands has been observed in different metallic systems[36–38] and it is part of a growth mechanism

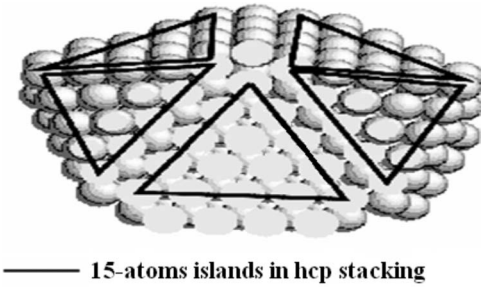

FIG. 8. Structure of a 286 atoms cluster.

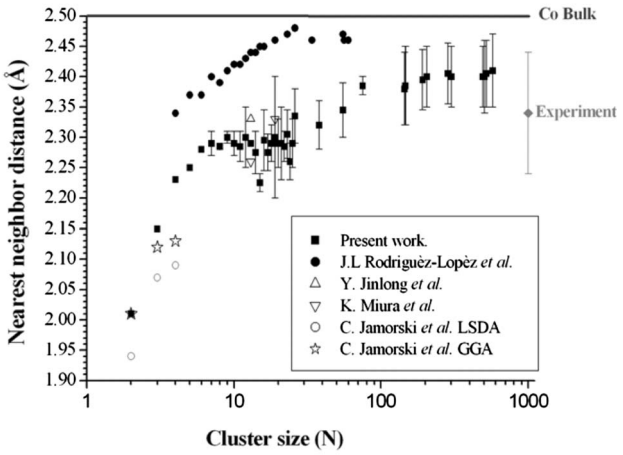

FIG. 9. Evolution of the computed nearest-neighbor distance with the cluster diameter. Our theoretical results are compared to the experimental point and to four different theoretical data: the semiemperical calculations by Rodríguez López *et al.* (Ref. 24), and the DFT calculations of Jamorski *et al.* (Ref. 40), Jinglong *et al.* (Ref. 41), and Miura *et al.* (Ref. 42).

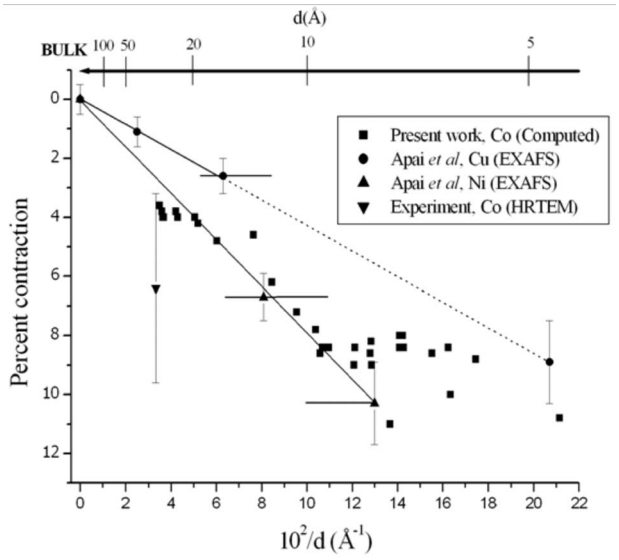

FIG. 10. Lattice contraction as a function of the inverse diameter $1/d$. Our experimental and simulation results for Co are compared to those by Apai *et al.*[43] for Ni and Cu.

which produces icosahedra from smaller decahedra. Finally, we note that recently Payne *et al.*[39] deduced a shell by shell growth pattern, which is in qualitative agreement with our findings.

2. Lattice parameter squeezing

Average interatomic and interplanar distances in our simulated structures are smaller than in bulk cobalt. A quantitative estimate of interatomic and interplanar distances has been obtained by calculating, for each cluster size, the average nearest-neighbor distance $\bar{a}$ (i.e., determining for each atom its nearest neighbor, calculating its distance, and averaging over all atoms). This distance is easily related to the distance between neighbor fcc (111) planes.

Figure 9 clearly shows that $\bar{a}$ increases with cluster size, i.e., there is a lattice parameter squeezing when the number of atoms decreases. For a four-atom cluster, $\bar{a}=2.23$ Å, whereas for a 574-atom cluster (diameter of ~2.9 nm), $\bar{a}=2.41$ Å. The analysis of the high resolution TEM (HRTEM) image of a 3 nm cobalt cluster (see Fig. 2) gives a distance between fcc (111) planes of 1.92 Å ±5%, which corresponds to an interatomic distance of 2.34 Å ±5%. This result is in good agreement with our calculations for clusters of the same size. We note that in fcc bulk, Co interatomic and interplanar distances are 2.50 and 2.05 Å, respectively.

Oscillations in the average nearest-neighbor distance are especially evident for small sizes, at which icosahedra are found for a large majority of nuclearities. For example, for $N=12-13$, there is a maximum in the average distance, which is followed by a decrease which reaches a minimum for $N=15$. This minimum is due to the undercoordinated atoms which begin to form the third icosahedral shell.

We can compare our results on lattice contraction to those of DFT calculations by Jamorski *et al.*[40] for clusters up to the tetramer, and to those by Jinlong *et al.*[41] and Miura *et al.*[42] for sizes of 13 and 19. The DFT results by Jamorski *et al.*[40] are obtained both in local spin density approximation and in generalized gradient approximation (GGA). From Fig. 9, it follows that our results and DFT results are in very good agreement with those of Jamorski *et al.*, especially to those obtained within the GGA approximation. For sizes of 13 and 19, our results agree well with those of Jinlong *et al.* and Miura *et al.* This demonstrates that our parametrization is able to reproduce bond-length contraction in good agreement with DFT calculations down to very low atomic coordination. In Fig. 9, we compare also our results with those by Rodríguez-López *et al.*,[24] obtaining that our lattice contractions are larger. This can be understood by the fact that, in the Gupta model potential, the contraction of the nearest-neighbor distance δ is ruled by the following equation, which expresses δ as a function of the number of nearest neighbors n_v of a given atom,[1]

$$\delta(n_v) = \frac{r(n_v) - r_0}{r_0} = \frac{1}{2(p-q)} \log\left(\frac{n_v}{12}\right), \tag{4}$$

where $r(n_v)$ is the optimal nearest-neighbor distance for the given number of nearest neighbors. From Eq. (4), it follows that the contraction is inversely proportional to $p-q$. In the parametrization of Ref. 24, $p-q$ is larger by a factor 1.5 than in our case. Therefore, we expect that our contractions will be larger than those of Ref. 24 approximately by the same factor. This prediction is very well confirmed in by the data reported in Fig. 9, especially for the smallest cluster sizes.

Finally, in Fig. 10, we report our simulation results about lattice contraction for Co as a function of $1/d$, with d diameter of the cluster, together with our experimental point, and with experimental data about contraction in Cu and Ni clusters, taken from Ref. 43. From Fig. 10, it follows that contraction in Co is quantitatively similar to contraction in Cu and Ni, with a behavior that, on average, is linear in $1/d$.

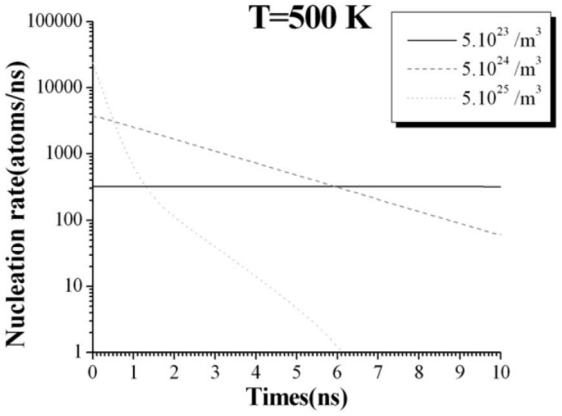

FIG. 11. Time evolution of the nucleation rate ζ for different initial densities at 500 K.

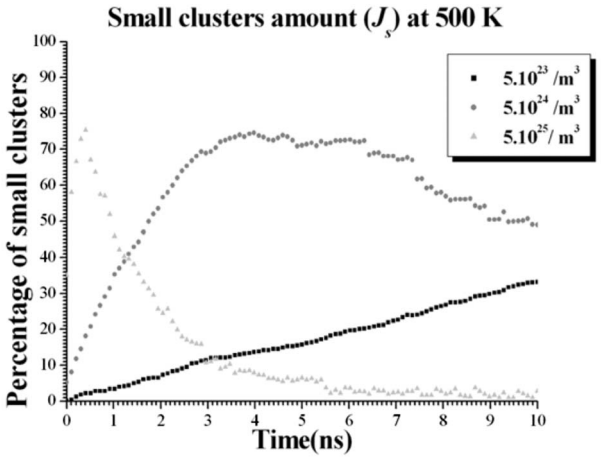

FIG. 12. Time evolution of J_s for different initial densities at 500 K.

This behavior can be rationalized as follows. Nearest-neighbor contraction is taking place for surface atoms. Therefore, the average contraction will be proportional to the ratio between the number of surface atoms and the total number of atoms, which scales as $1/d$ for sufficiently large clusters.

C. Growth mechanism

Computation allows us to investigate the effect of pressure and temperature on the cluster growth mechanisms. The main objective of this study is to provide a useful guideline to adjust and optimize the working parameters of the cluster generator in order to improve the control of the aggregate size. Indeed, the knowledge of the cluster size distribution at a given time and for fixed temperature and pressure can provide information to determine laser fluence, triggering delay of the helium puff, upstream gas pressure, and nozzle design. Consequently, a study has been undertaken to examine the evolution with time of the cluster growth and the occurrence of the different regimes of growth as a function of particle density and temperature.

1. Density effect

The initial density in monomers is expected to be a crucial parameter for the evolution of the nucleation rate. Indeed, the higher the concentration is, the more the monomers have the opportunity to nucleate or to meet an already formed small cluster. The evolution of the nucleation rate ζ is plotted in Fig. 11, and the onset of the coalescence regime is investigated by studying the variation of the number of small clusters J_s with time (see Fig. 12). The temperature is kept constant for the different simulations, only the density changes. Three different densities are used: 5×10^{23}, 5×10^{24}, and 5×10^{25} atoms/m^3. If one considers a temperature of 500 K, these densities are approximately equivalent to pressures of 30, 300, and 3 bar, respectively. These correspond to experiments in low, normal, and high pressure regimes.

The nucleation rate changes by several order of magnitude depending on density and follows approximately an exponential decay law, with the exception of the case of $n_0=5\times10^{25}$ atoms/m^3, in which there are two kinds of exponential decays, a fast one before 1.3 ns and a slower one between 1.3 and 6 ns. For an initial density of 10^{23} atoms/m^3, the nucleation rate has a constant value of about 320 atoms/ns. At 5×10^{24} atoms/m^3, ζ ranges from nearly 3700 to 60 atoms/ns, while for $n_0=5\times10^{25}$ atoms/m^3, the decay is more important, the value of ζ going from 24 000 to 1 atoms/ns at 6 ns afterward the monomers amount is nearly depleted. The two exponential decay regimes of the nucleation rate at $n_0=5\times10^{25}$ atoms/m^3 can be explained by the rarefaction of monomers with time.

The analysis of the plot of J_s with time provides information about the different regimes of clusters growth: the nucleation regime by aggregation of monomers and the coalescence regime in which the fusion of small clusters can take place.

In the case of $n_0=5\times10^{23}$ atoms/m^3 the evolution of the concentration of small clusters is linear thus the regime of cluster growth is to a large extent a nucleation regime. At initial densities of 5×10^{24} and 5×10^{25} atoms/m^3, the time evolution of the quantity of small clusters attains a maximum at, respectively, 4 and 0.4 ns. Before this maximum, the regime is essentially a nucleation one. After the maximum, aggregation, it is dominated by coalescence.

2. Temperature effect

The effect of the temperature is more complex and weaker than the density effect. A higher temperature allows the monomers to meet faster but makes the bond less stable. A higher temperature increases also the coalescence rate of small clusters.

The dependence with time of ζ (Fig. 13) and J_s (Fig. 14) is drawn at a constant density of 5×10^{24} atoms/m^3 and for 300, 400, 500, 600, 700, and 800 K. For temperatures of 300 and 400 K, the nucleation rate has nearly the same value; it decreases from 350–360 to 7–8 atoms/ns. For 500, 600, and 800 K, the nucleation decreases from, respectively, 470,

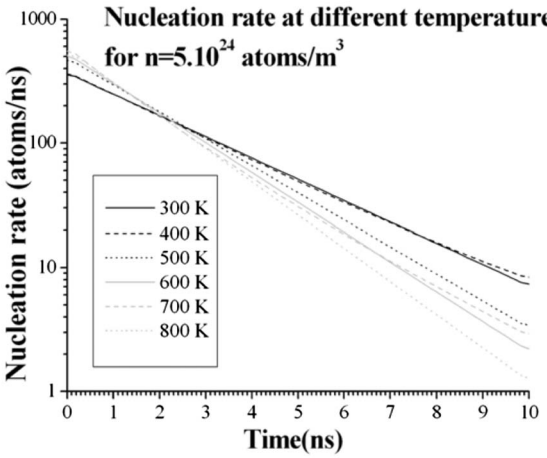

FIG. 13. Time evolution of ζ at different temperatures at an initial density of 5×10^{24} atoms/m^3.

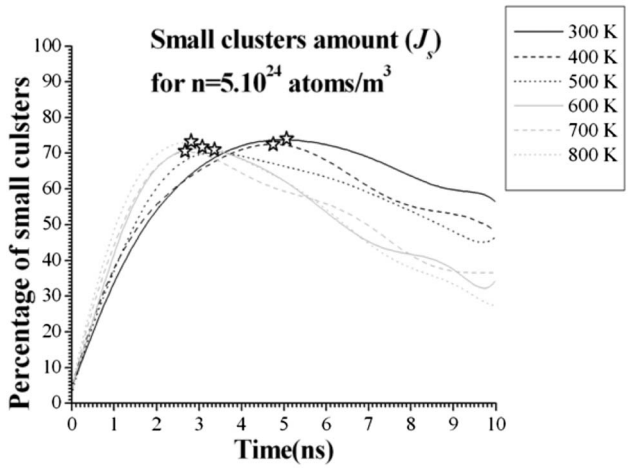

FIG. 14. Time evolution of J_s at different temperatures at an initial density of 5×10^{24} atoms/m^3. Stars depict the maximum value.

500, and 515 to 3.4, 2.2, and 1.2 atoms/ns, but at 700 K, ζ diminishes from 550 to 2.9 atoms/ns. Therefore, the initial nucleation rate seems to increase with temperature, whereas the final rate is decreasing with temperature except at 700 K where the initial nucleation rate is slightly higher than at 800 K and the final nucleation rate is higher than the value at 600 K. The inversion of trend occurs between 2 and 3 ns.

The increase of the nucleation rate with temperature is expected due to the increasing mobility of monomers and clusters. However, when temperature becomes very high, bond breaking events in very small clusters (dimers, for example) begin to become likely. This can be the cause of the decrease of the nucleation rate which is observed at 800 K. The maximum of J_s is at 2.7, 2.8, 3, and 3.5 ns for, respectively, 700, 800, 600, and 500 K, and at 4.7 and 4.9 ns for, respectively, 400 and 300 K. Hence, there is a slow coalescence regime at 300 and 400 K and a faster regime between 500 and 800 K. The latter is mainly due to the increased mobility of aggregates.

V. CONCLUSIONS

In summary, the geometric structure of cobalt clusters has been investigated with MD simulations by growing atom by atom from a small seed up to the size of 600 atoms. The structure follows mainly an icosahedral or a decahedral pattern with fcc-like facets and islands in stacking fault position. The structures obtained in the size range $N\leqslant55$ have been compared to previous DFT and semiempirical calculations,[24,35] obtaining agreement for almost all cases. Kinetic trapping effects have been demonstrated to take place also in the small-size range for some nuclearities as $N=38$. These effects are thus expected to be important for large sizes.

The contraction of the nearest-neighbor distance has been investigated as a function of cluster size, finding, for small cluster sizes ($N\leqslant18$), a good agreement with previous DFT calculations by different groups.[40–42] The behavior of the contraction at larger sizes has been compared to an experimental results obtained for a cluster generated by laser ablation, obtaining again a good agreement. On the other hand, the comparison with previous semiempirical calculations[24] for cluster sizes $N\leqslant55$ has revealed some quantitative discrepancy, which has been rationalized in terms of the parameters of the two semiempirical models. Finally, the evolution of the growth process of clusters from a vapor of isolated atoms has been simulated for different vapor densities and temperatures. Nucleation and coalescence regimes have been identified.

[1] F. Baletto and R. Ferrando, Rev. Mod. Phys. **77**, 371 (2005).
[2] J. A. Alonso, Chem. Rev. (Washington, D.C.) **100**, 637 (2000).
[3] E. Cottancin, J. Lermé, M. Gaudry, M. Pellarin, J.-L. Vialle, M. Broyer, B. Prével, M. Treilleux, and P. Mélinon, Phys. Rev. B **62**, 5179 (2000).
[4] A.-C. Dupuis, Prog. Mater. Sci. **50**, 929 (2005).
[5] B. Berkovsky and V. Bashtovoy, *Magnetic Fluids and Applications Handbook* (Begell Home, Inc., New York, 1996).
[6] T. P. Martin, Phys. Rep. **273**, 199 (1996).
[7] F. Dumas-Bouchiat, Ph.D. thesis, Limoges University, 2005.
[8] S. H. Baker, S. C. Thornton, K. W. Edmonds, M. J. Maher, C. Norris, and C. Binns, Rev. Sci. Instrum. **71**, 3178 (2000).
[9] H. R. Siekmann, Ch. Lüder, J. Faehrmann, H. O. Lutz, and K. H. Meiwes-Broer, Z. Phys. D: At., Mol. Clusters **20**, 417 (1991).
[10] P. M. Denby and D. A. Eastham, Appl. Phys. Lett. **79**, 2477 (2001).
[11] K. Sakaguchi, K. Mihama, and Y. Saito, J. Appl. Phys. **70**, 5049 (1991).
[12] R. A. Ganeev, M. Baba, A. I. Ryasnyanski, M. Suzuki, and H. Kuroda, Opt. Commun. **240**, 437 (2004).

[13] M. Vitiello, S. Amoruso, C. Altucci, C. de Lisio, and X. Wang, Appl. Surf. Sci. **248**, 163 (2005).
[14] F. Baletto, C. Mottet, and R. Ferrando, Phys. Rev. Lett. **84**, 5544 (2000).
[15] G. Rossi, A. Rapallo, C. Mottet, A. Fortunelli, F. Baletto, and R. Ferrando, Phys. Rev. Lett. **93**, 105503 (2004).
[16] E. Aprà, F. Baletto, R. Ferrando, and A. Fortunelli, Phys. Rev. Lett. **93**, 065502 (2004).
[17] W. C. Swope, H. C. Andersen, P. H. Berens, and K. R. Wilson, J. Chem. Phys. **76**, 637 (1982).
[18] F. Cleri and V. Rosato, Phys. Rev. B **48**, 22 (1993).
[19] C. Mottet (private communication).
[20] A. C. Andersen, J. Chem. Phys. **72**, 2384 (1980).
[21] F. Baletto, R. Ferrando, A. Fortunelli, F. Montalenti, and C. Mottet, J. Chem. Phys. **116**, 3856 (2002).
[22] M. B. Torres, E. M. Fernandez, and L. C. Balbas, Phys. Rev. B **71**, 155412 (2005).
[23] J. Rogan, G. Garcia, C. Loyola, W. Orellana, R. Ramirez, and M. Kiwi, J. Chem. Phys. **125**, 214708 (2006).
[24] J. L. Rodríguez-López, F. Aguilera-Granja, K. Michaelian, and A. Vega, Phys. Rev. B **67**, 174413 (2003).
[25] D. Faken and H. Jónsson, Comput. Mater. Sci. **2**, 279 (1994).
[26] F. Dumas-Bouchiat, C. Champeaux, H. S. Nagaraja, F. Rossignol, N. Lory, A. Catherinot, P. Blondy, and D. Cros, Thin Solid Films **453-454**, 296 (2004).
[27] T. G. Dietz, M. A. Duncan, D. E. Powers, and R. E. Smalley, J. Chem. Phys. **74**, 6511 (1981).
[28] R. E. Smalley, Laser Chem. **2**, 167 (1983).
[29] P. Milani and W. A. de Heer, Rev. Sci. Instrum. **61**, 1835 (1990).
[30] F. Dumas Bouchiat, H. S. Nagaraja, F. Rossignol, C. Champeaux, and A. Catherinot, Appl. Surf. Sci. **247**, 76 (2005).
[31] A. Perez, P. Mélinon, V. Paillard, V. Dupuis, P. Jensen, A. Hoareau, J. P. Perez, J. Tuaillon, M. Broyer, J. L. Vialle, M. Pellarin, B. Baguenard, and J. Lerme, Nanostruct. Mater. **6**, 43 (1995).
[32] G. Rossi, A. Rapallo, C. Mottet, A. Fortunelli, F. Baletto, and R. Ferrando, Phys. Rev. Lett. **93**, 105503 (2004).
[33] G. Rossi and R. Ferrando, Chem. Phys. Lett. **423**, 17 (2006).
[34] F. Baletto, A. Rapallo, G. Rossi, and R. Ferrando, Phys. Rev. B **69**, 235421 (2004).
[35] Q. M. Ma, Y. Liu, Z. Xie, and J. Wang, J. Phys.: Conf. Ser. **29**, 163 (2006).
[36] F. Baletto and R. Ferrando, Surf. Sci. **490**, 361 (2001).
[37] F. Baletto, C. Mottet, and R. Ferrando, Phys. Rev. B **63**, 155408 (2001).
[38] J. L. Rodríguez-López, J. M. Montejano-Carrizales, U. Pal, J. F. Sánchez-Ramírez, H. E. Troiani, D. García, M. Miki-Yoshida, and M. José-Yacamán, Phys. Rev. Lett. **92**, 196102 (2004).
[39] F. W. Payne, W. Jiang, J. W. Emmert, J. Deng, and L. A. Bloomfield, Phys. Rev. B **75**, 094431 (2007).
[40] C. Jamorski, A. Martinez, M. Castro, and D. R. Salahub, Phys. Rev. B **55**, 10905 (1997).
[41] Jinlong Yang, Chuanyum Xiao, Shangda Xia, and Kelin Wang, Phys. Rev. B **48**, 12155 (1993).
[42] K. Miura, H. Kimura, and S. Imanaga, Phys. Rev. B **50**, 10335 (1994).
[43] G. Apai, J. F. Hamilton, J. Stohr, and A. Thompson, Phys. Rev. Lett. **43**, 165 (1979).